DOI: 10.1002/ejic.200901105

Synthesis and Characterization of Metallic Co with Different Hierarchical Structures Prepared by a Simple Solvothermal Method

Lianfeng Duan,[a] Shusheng Jia,[a] and Lijun Zhao*[a]

Keywords: Hierarchical structures / Crystal growth / Cobalt / Magnetic properties

Magnetic metallic cobalt with different hierarchical structures, such as dendritic particles, flowery particles, and flocky spheres, has been successfully prepared by using a simple solvothermal process in which the relative amounts of $H_2C_2O_4$ and $N_2H_4{\cdot}H_2O$ in the reaction system were rationally adjusted. The Co crystals with hierarchical structure had a hexagonal-close-packed (hcp) structure. The dendritic Co crystal comprises several 1–5 μm long dendrites, and the hierarchical assemblies radiate from the center. The flowerlike Co submicrocrystals are composed of petal-like crystals around 1.5 μm in diameter and 100–200 nm thick. Interestingly, an intergrade from single-crystal to polycrystalline structures for flowerlike Co submicrocrystals is observed. The flocky spheres, about 600 nm in diameter, consist of 5 nm thick nanosheets. In addition, a growth mechanism is proposed which is based on the evolution of the structure and morphology with increasing reaction time. Further magnetic measurements for the Co crystals with different hierarchical structures indicated that the morphology of the Co crystals had an obvious influence on their magnetic properties.

Introduction

Magnetic materials have attracted considerable interest due to their novel properties and many applications in magnetic recording media, sensors, and other devices.[1–4] Cobalt compounds display a wealth of magnetic, electronic, optical, microwave, and catalytic properties.[5–9] It is believed that the properties of micro-/nanomaterials strongly depend on their size, shape, and dimensionality. Because the multiple crystal structures [such as hexagonal-close-packed (hcp), face-centered-cubic (fcc), and ε-phase][10] and morphologies of cobalt have a significant influence on its properties, there has been an increasing number of reports on the synthesis of cobalt with various shapes. Nanorods, micro-/nanowires, nanofibers, nanobelts, nanotubes, nanorings, nanodisks/nanoplatelets,[11–15] two- and three-dimensional superlattices, and chain-like structures[16] have been successfully synthesized. In this contribution, not only do we study the transformation of morphologies, but we also focus attention on an intergrade from single-crystal to polycrystalline hierarchical structures synthesized by the solvothermal method.

To date, various synthetic methods, including thermal decomposition of organometallic precursors, electrodeposition technology, templated/mediated synthesis, electrospinning techniques, magnetic-field-induced processes, and hydro-/solvothermal methods, have been developed to fabricate cobalt.[17–25] As one of the most common liquid-phase methods, the hydro-/solvothermal method is often used to prepare high-purity materials and to control the product morphology.[26] Anisotropic magnetic particles or superstructures are expected to exhibit interesting magnetic properties such as enhanced coercivity. Hence, it has recently become a hot topic to fabricate magnetic materials with hierarchical structures. Here, we report a tunable, facile, and surfactant-free solvothermal synthesis of Co microcrystals possessing a variety of hierarchical structures. By controlling the content of $H_2C_2O_4$ in the reaction system, we obtained Co products with different sizes and morphologies. Likewise, the effects of $N_2H_4{\cdot}H_2O$ were studied under conditions of fixed alkalinity. Moreover, the magnetic properties of the Co products obtained at different conditions were investigated to explore the dependence of the magnetic properties on the sizes and morphologies of the particles.

Results and Discussion

Figure 1a shows XRD patterns of as-prepared cobalt crystals (S1, S2, and S3). All of them are well crystallized. The diffraction peaks for the as-formed samples at 2θ = 41.68, 44.24, 47.44, and 75.89°, which match the reflection planes of (100), (002), (101), and (110), respectively, could be indexed to a pure hcp cobalt phase (JCPDS 05-0727). Trace carbon peaks (JCPDS 26-1076) can also be observed, which are derived from $C_2O_4^{2-}$ ions formed during the solvothermal process. However, it is observed that the intensities of these reflections do not agree with those in the

[a] Key Laboratory of Automobile Materials (Jilin University), Ministry of Education and School of Materials Science and Engineering, Jilin University,
Changchun 130022, China
Fax: +86-431-85095876
E-mail: lijunzhao@jlu.edu.cn

Supporting information for this article is available on the WWW under http://dx.doi.org/10.1002/ejic.200901105.

PDF card (JCPDS 05-0727). For instance, in the card, the diffraction peak of (101) is the strongest, whereas the (002) peak is weaker. However, the relative intensity of the (002) peak for the samples prepared under solvothermal conditions increases significantly, which might result from the oriented aggregation of the crystallites along the *c* axis. To determine the content of Co, energy dispersive X-ray spectroscopy (EDS) was carried out on the S2 sample, and the result is shown in Figure 1b, where strong Co peaks and weak C peaks are observed. By calculation, the Co content in the S1, S2, and S3 samples should be 98.5%, 92.6%, and 97.6%, respectively. Note that Si, also observed in the EDS spectrum, is due to the silicon wafer supporting the sample.

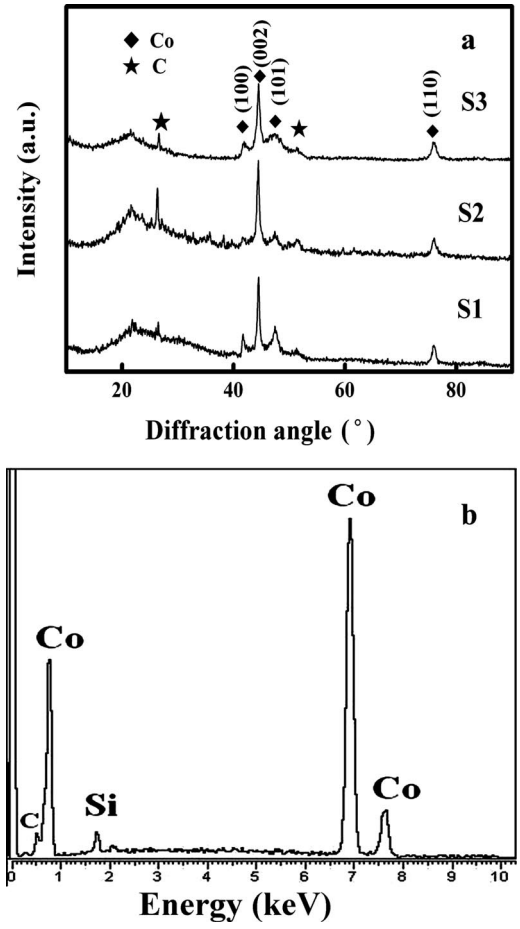

Figure 1. (a) XRD patterns of the as-obtained products S1, S2, S3 (diamonds represent cobalt; pentagrams indicate carbon) and (b) EDS pattern of S2.

Figure 2a is a typical low-magnification SEM image of S1, from which we can observe that novel and large-scale dendritic superstructures with an average diameter of approximately 10 μm were fabricated. A higher-magnification SEM image of an individual crystallite of S1 indicates that the superstructures comprise several dendrites having hierarchical assemblies that radiate from the center (Figure 2b). The final product consists of many dendritic architectures with lengths of 1–5 μm along the trunks, as can be seen from the SEM images displayed in Figures 2a and b. Further insight into the morphology and microstructure of hierarchical Co structures was gained by using TEM and high-resolution TEM (HRTEM). Figure 2c shows the TEM image of the as-prepared S1 sample. Figure 2d is the corresponding selected area electron diffraction (SAED) pattern, which illustrates the single-crystal nature of the cobalt dendrite. Some elongated diffraction spots in the SAED can be seen because of the deformation of several branches in the metallic cobalt superstructures. Furthermore, the SAED spots can be consistently indexed to (101), (103), and (002) facets, in good agreement with the XRD data. The HRTEM image of the arrow tip of the dendrite (Figure 2c) is shown in Figure 2e. From this figure, the lattice interplanar spacing is measured to be 0.20 nm, corresponding to the (002) plane of hcp Co. The [001] direction, corresponding to the (002) plane of hcp Co, as shown in Figure 2e, is parallel to the growth direction of the main branch, as displayed by the arrow in Figure 2c, indicating that this growth is along the [001] direction.

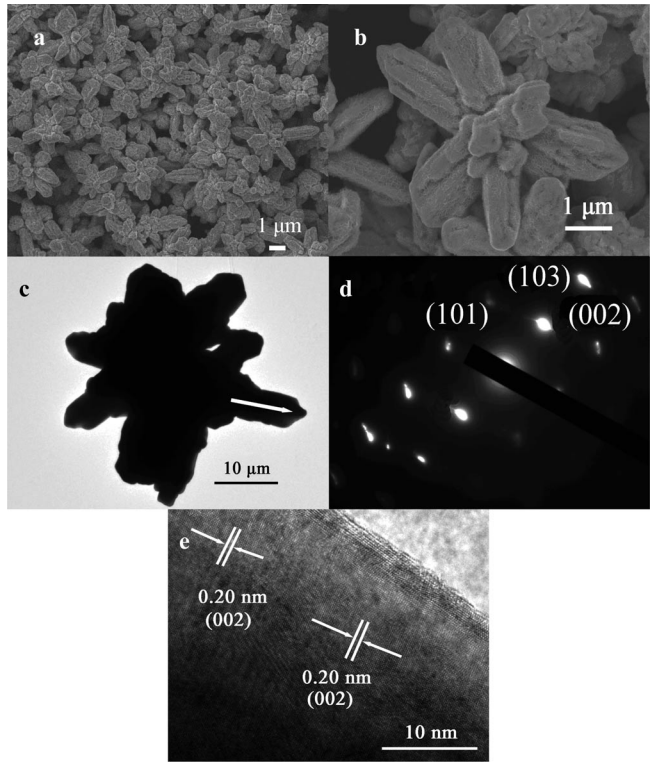

Figure 2. (a) Low-magnification SEM, (b) high-magnification SEM, (c) TEM, (d) SAED, and (e) HRTEM images of S1.

To investigate the effect of $N_2H_4 \cdot H_2O$ on the morphology, the as-prepared S2 sample was examined by SEM. Figure 3a shows the overall morphology of S2, which indicates that the products mainly consist of flowerlike structures. The high-magnification image of a single Co submicrocrystal with a size of about 1.5 μm demonstrates that the architecture is constituted by a few petals with sizes of 100–200 nm radiating from the center (Figure 3b). The morphology of the flowerlike Co is further determined by TEM (Figure 3c), and is consistent with that observed by SEM. The SAED pattern (Figure 3d) illustrates the imperfect single-crystal nature of the cobalt, where some separated and

elongated diffraction spots are observed. An unusual HRTEM image (Figure 3e) was recorded on the fringe of the S2 sample. From Figure 3e, the lattice interplanar spacings are measured to be 0.22 nm, corresponding to the (100) plane of hcp Co in the "A" area. In the "B" area, the lattice interplanar spacings are measured to be 0.20 nm, corresponding to the (002) plane of hcp Co. In order to understand the unusual HRTEM image, we have drawn an explanatory diagram in Figure 3f. The grain boundary separating the crystals having different crystallographic orientations in polycrystalline materials is shown in Figure 3f. Within the boundary region, which is just several atoms wide, there is some atomic mismatch in a transition from the crystalline orientation of one grain to that of an adjacent one. This orientation mismatch is slight, in the order of a few degrees, so the term small- (or low-) angle grain boundary is used.[27] These boundaries can be described in terms of dislocation arrays. One simple small-angle grain boundary is formed when edge dislocations are aligned in the manner shown in Figure 3f. The angle of misorientation, θ, is indicated in the formula $\theta \approx \mathrm{tg}\theta = \mathbf{b}/D \approx 11°$, where **b** is the Burgers vector and D is the interval of adjacent defect.

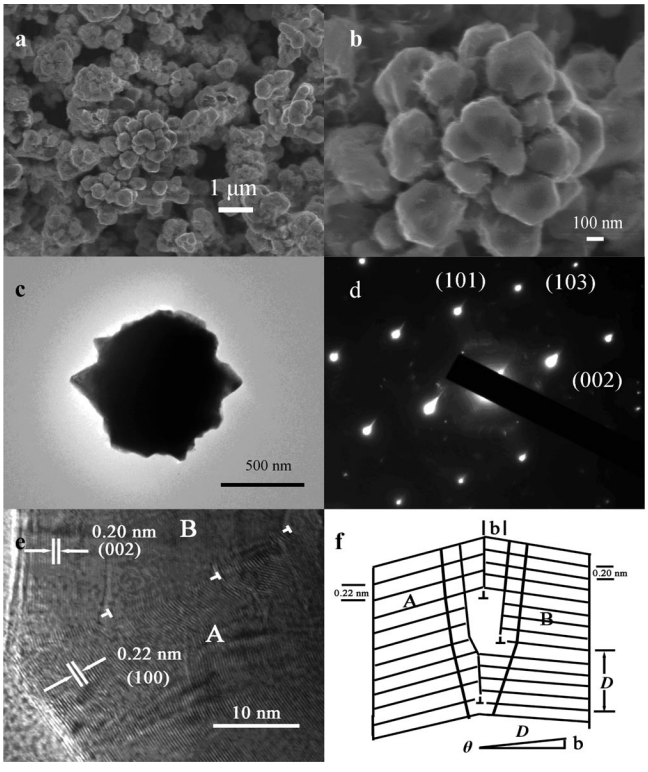

Figure 3. (a) Low-magnification SEM, (b) high-magnification SEM, (c) TEM, (d) SAED, and (e) HRTEM images of S2; (f) demonstration of HRTEM images of S2.

This is different from the twin structure, which could form as a result of the erroneous attachment of atoms to a growing crystal in such a way that two crystals appear to be growing out of each other, such as in gold and silver.[28] Hence, flowerlike structures may be a transitional morphology from single-crystal to polycrystalline.

The effect of $H_2C_2O_4$ on the morphology was also researched. The S3 sample is composed of flocky spheres about 600 nm in diameter (Figure 4a). A high-magnification SEM image (Figure 4b) displays the detailed structure of the spheres. These comprise a number of nanosheets with an average thickness of about 5 nm, as estimated from the standing nanosheets in the SEM image. Figure 4c shows a TEM image of an individual flocky sphere. The corresponding SAED pattern (Figure 4d) denotes that the Co nanosheets are polycrystalline. According to the interplanar spacing of the hexagonal Co, the (100), (002), (101), (102), (110), (103), and (112) planes could be determined. The SAED results are in good agreement with the XRD data. To depict the nature of the as-prepared S3 product, HRTEM was also performed, and the micrograph is shown in Figure 4e. The inner lattice fringes of S3 can be seen clearly in Figure 4e . The interplanar spacing was measured to be 0.22 nm, corresponding to the (100) planar spacing of hcp Co. However, the inner lattice fringes of S3, shown in Figure 4e, are in every orientation. In conclusion, the S3 sample is composed of a single-crystalline sub-micro spherical core and polycrystalline nanosheets. It was also found that the nanosheet was not single-layered, rather composed of randomly attached smaller sheets.

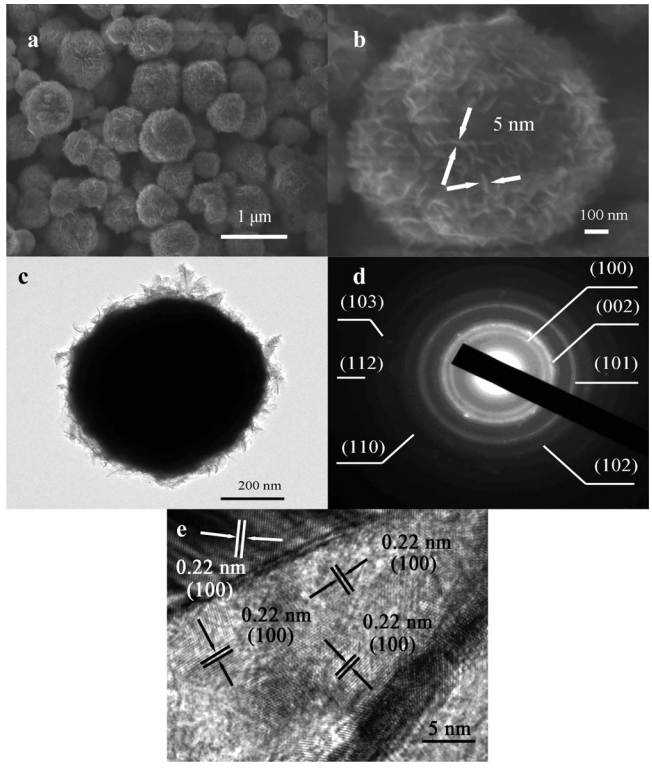

Figure 4. (a) Low-magnification SEM, (b) high-magnification SEM, (c)TEM, (d) SAED, and (e) HRTEM images of S3.

To shed light on the growth processes of the hierarchical Co structures, we studied the products (obtained at different stages of the reaction under 200 °C solvothermal treatment), as shown in Figure 5 and Figures S1–S3 (Supporting Information). After 6 h of solvothermal treatment, the S1 samples obtained were composed of irregular par-

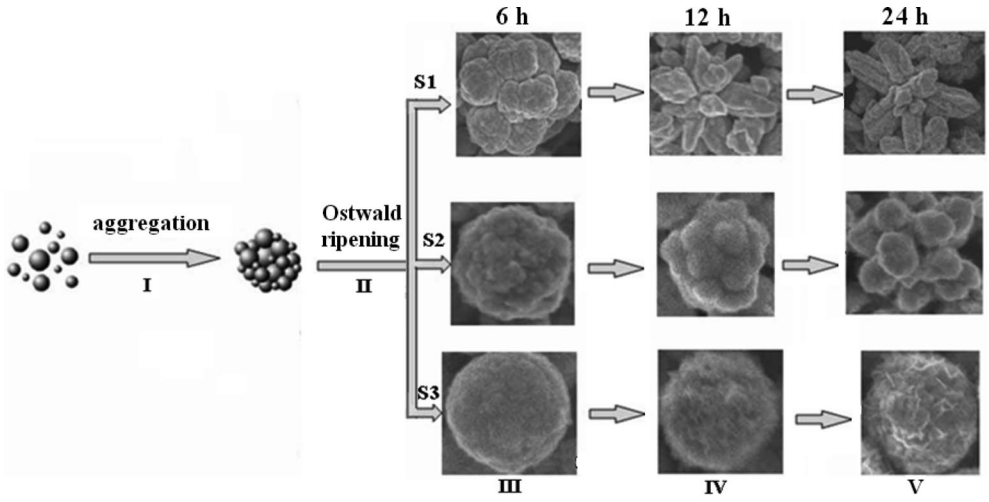

Figure 5. Schematic illustration of how the hierarchical structures of the Co crystals vary with solvothermal treatment time.

ticles approximately 5 μm in size. The complete conversion of the flowerlike congeries to dendritic Co through the growth of the microparticles can be achieved after 12 h of solvothermal treatment. After 24 h of solvothermal treatment, large-scale dendritic Co microcrystals were obtained. S2 with accidented surfaces appeared after 6 h of solvothermal treatment. Note that the average diameter of the protuberances was 20 nm. Increasing the reaction time to 12 h in the same reaction system led to samples containing spherical nano-protuberances with average diameters of 50 nm. After 24 h of solvothermal reaction, flowery S2 samples were entirely composed of petals of approximately 400 nm. For S3, after 12 h of solvothermal treatment, flakelets were present. The hierarchical nanosheets were clearer and more complete on increasing the treatment time to 24 h.

On the basis of the above experimental observations, we have easily obtained three kinds of hierarchical architectures. The formation process of the hierarchical structures can be seen clearly in Figure 5. The preparation of metal Co probably involves the following chemical reactions:

$$Co^{2+} + H_2C_2O_4 \rightarrow Co(COOH)_2 \quad (I)$$

$$Co(COOH)_2 + 2(CH_2OH)_2 + 8OH^- \rightarrow Co(CH_3COO)_2 + 2CO_2 + 8H_2O \quad (II)$$

$$Co(CH_3COO)_2 + 14OH^- \rightarrow CoC_2O_4\downarrow + 2CO_2 + 10H_2O \quad (III)$$

$$CoC_2O_4 + (CH_2OH)_2 + 10OH^- \rightarrow Co + 4CO_2 + 8H_2O \quad (IV)$$

$$CoC_2O_4 + N_2H_4 + 4OH^- \rightarrow Co + N_2 + C_2O_4^{2-} + 4H_2O \quad (V)$$

The chemical reactions involved in the formation of S1 and S3 are described by reactions (I), (II), (III), and (IV) above, whereas S2 is obtained as described by reactions (I), (II), (III), and (V).

Small particles are formed by a conventional nucleation process at stage I. These then diffuse and aggregate to decrease their high surface energies. Moreover, the $Co(COOH)_2$ molecules containing carboxyl groups tend to agglomerate into spherical clusters as a result of the steric effect and hydrophilicity of the carboxylate.[29,30] Furthermore, polyols are strong complexing and reducing agents at high temperatures under basic conditions and certainly play a role in the formation of the Co nanoparticles. The solid intermediate phase $Co(CH_3COO)_2$ is obtained from the reaction mixture at the beginning of the reduction.[31] At stage II, with the continuous advancement of the reaction, assembled nanoparticles with a relatively large size might serve as crystallization nuclei. The thermodynamically active sites, such as surface defects and active crystal surfaces, are generated on the first Co nuclei formed as a result of the solvation of the Co surface.[32] These active sites can then serve as heterogeneous nucleation sites. Once nuclei are formed at these active sites, growth with preferential orientation can start. When the reactants are consumed because of particle growth, the larger ones have smaller surface free energies and consequently grow at the cost of the smaller ones, following a typical Ostwald ripening process.[33] It was reported that the morphology and size of the products depend on the competition between crystal nucleation and crystal growth, and the pH value has an impact on both of these factors.[34]

Compared with that of S1 at stage III, the surface of S2 is smoother. As mentioned above, S1 is composed of irregular particles of approximately 5 μm, whereas the average diameters of the protuberances on the surface of S2 are about 20 nm. Hence, we speculate that the addition of $N_2H_4{\cdot}H_2O$ can influence the roughness of the surface of the Co microcrystals to some extent. Complexation of $N_2H_4{\cdot}H_2O$ with Co^{2+} ions will decrease the concentration of Co^{2+} ions available for the formation of CoC_2O_4. More nuclei can always be formed at a higher Co^{2+} concentration due to a higher crystal growth rate, so particles with smaller sizes can be obtained at higher Co^{2+} concentrations. As a result, more smaller building blocks can aggregate into microspheres with smooth surfaces at higher Co^{2+} concentrations, as observed for S2; on the contrary, in the formation of S1, fewer particles of a larger size form microspheres with rough surfaces. Comparing S1 and S2 at stages IV and

V, we can see that dendritic S1 and flowerlike S2 are formed. Here, the addition of $N_2H_4{\cdot}H_2O$ may accelerate the growth of S1, because of its strong reducing ability. The rapid growth of S1 may make the 5 μm irregular particles grow into dendritic shapes, whereas the relatively slow growth of S2 may only give an opportunity for the 20 nm protuberances to grow.

At stage III, the surface of S3 is also smoother than that of S1. As mentioned above, the double dosage of $H_2C_2O_4$ may play a key role. At stages IV and V, the reduction potential in solution for S1 is higher than that for S3, because a double amount of $H_2C_2O_4$ is used for the preparation of S3 in the reaction system. Higher pH values facilitate the reduction process for the preparation of Co in ethylene glycol (EG). Hence, the low reduction potential in solution leads to the slower reduction rate, which causes the Co spherical clusters to become the reactive core of the flakelets. In this case, the interaction between inorganic materials and the abundant $H_2C_2O_4$ was the main driving force for self-assembly.

We conclude that the formation of Co hierarchical architectures is controlled by the rates of nucleation and growth. $H_2C_2O_4$ plays an important role in determining the nucleation rate, while the growth speed is under the control of $N_2H_4{\cdot}H_2O$. We successfully fabricated different Co hierarchical architectures by adjusting the dosages of $H_2C_2O_4$ and $N_2H_4{\cdot}H_2O$. Furthermore, the reaction systems of S2 and S3 show lower pH values relative to that of S1. Hence, the rate of crystal nucleation was slower than that of crystal growth in the reaction systems of S2 and S3, relative to that for S1. The above explanation may be the reason why the particle sizes of S1 are larger than those of S2 and S3.

To investigate the dependence of the morphologies on the magnetic properties of Co hierarchical architectures, magnetization measurements were performed. Figure 6 shows the hysteresis loops of S1, S2, and S3 measured in fields between ±1 T at room temperature.

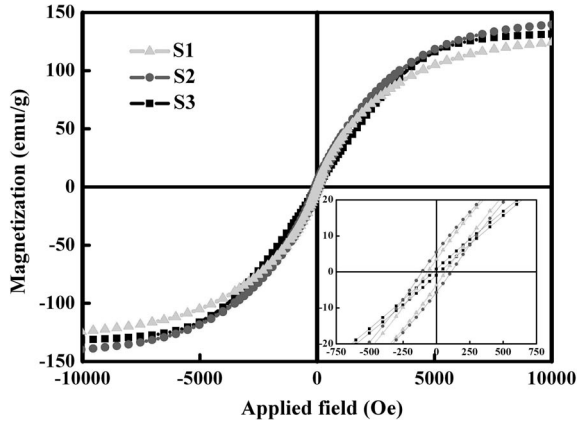

Figure 6. Magnetization curve measured at room temperature for (a) S1, (b) S2, (c) S3.

The magnetic parameters obtained from Figure 6 are listed in Table 1. The values of saturation magnetization (M_s) are 124, 139, and 131 emu/g; the values of remnant magnetization (M_r) are 3.6, 5.4, and 0.9 emu/g; and the values of coercivity (H_c) are 75, 105, and 22 Oe for S1, S2, and S3, respectively. Experimental errors may be responsible for the different M_s values of the samples. For S2, $N_2H_4{\cdot}H_2O$ is not added into the reaction; therefore, the growth of Co particles is relatively slow, which facilitates complete crystallization. Hence, S2 has the highest M_s value. Furthermore, a double dosage of $H_2C_2O_4$ was used to fabricate S3, which would decrease the reducing rate of Co and make for complete crystallization to some extent. S2has a higher M_s value relative to S1. However, Co hierarchical structures generally exhibit enhanced values, which may be contributed to their hierarchical architectures. The boundary dislocation arrays of S2 may be the main reason for its highest M_r and H_c. However, the coercivity of S3 was much lower than those of S1 and S2 by the reduced influence of its architecture on the rotation of magnetic dipoles. Generally, an increased amount of energy (or higher magnetic field strength) is required to change the direction of magnetization of these aligned dipoles, which suggests larger coercivity for S1 and S2, as observed. The difference of Co contents between S1 and S2 is another reason for the lower H_c value of S1. Furthermore, such a decrease could also be ascribed to the special 3D assembled structure of S3, which is an integral crystallite possessing low anisotropy.[35] Compared with S1 and S2, S3 may have the lowest shape anisotropy. Because elliptic morphology has the lowest shape anisotropy, the morphologies of S3 are closer to an ellipse. Hence, S3 has the lowest M_r and H_c.

Table 1. Magnetic parameters obtained from hysteresis loops.

Samples	S1	S2	S3
M_s (emu/g)	124	139	131
M_r (emu/g)	3.6	5.4	0.9
H_c (Oe)	75	105	22

Conclusions

In summary, magnetic metallic Co samples with different hierarchical architectures, such as dendritic particles, flowery particles, and flocky nanospheres, have been successfully prepared by using a simple solvothermal process and adjustment of the dosages of $H_2C_2O_4$ and $N_2H_4{\cdot}H_2O$ in the reaction solution. Among the three hierarchical architectures, we can observe the transformation from single-crystal to polycrystalline structures for flowerlike Co submicrocrystals. Moreover, magnetic measurements indicate that the magnetic properties of Co hierarchical architectures depend on their morphologies.

Experimental Section

All reagents were analytical grade commercial products used without purification. Detailed experimental parameters and corresponding brief results are listed in Table 2.

In the first step, $CoCl_2{\cdot}6H_2O$ (0.2 g) was dissolved in EG (20 mL) with magnetic stirring at room temperature for 20 min. Quantified

Table 2. Brief summary of the experimental parameters and corresponding results.

Sample	$H_2C_2O_4$ (g)	NaOH (g)	$N_2H_4{\cdot}H_2O$ (mL)	Co content (%)	Morphology
S1	0.05	0.2	2	98.5	dendritic particles
S2	0.05	0.2	0	92.6	flowery particles
S3	0.1	0.2	2	97.6	flocky spheres

$H_2C_2O_4$ and NaOH were added to the solution, and then $N_2H_4{\cdot}H_2O$ (2.0 mL, 55 vol% analytical reagent) was added dropwise at room temperature followed by vigorous stirring for 20 min. Subsequently, the solution was transferred into a 30 mL Teflon-lined stainless steel autoclave. The autoclave was sealed and maintained at 200 °C for 24 h and then cooled to room temperature naturally. The products (S1, S2, and S3) were collected by filtration, washed several times with distilled water and absolute ethanol, and finally dried in a vacuum oven at 60 °C for 4 h.

The phases were identified by means of XRD with a Rigaku D/max 2500pc X-ray diffractometer with Cu-K_α radiation (λ = 1.54156 Å) at a scan rate of 0.04°S^{-1}. The morphologies were characterized with a JEOL JSM-6700F field-emission scanning electron microscope (FESEM) operated at an acceleration voltage of 8.0 kV and equipped with an energy dispersive X-ray spectrometer (EDS). TEM, HRTEM observations and selected area electron diffraction (SAED) patterns were carried out with a JEOL 2100F instrument with an emission voltage of 200 kV. Magnetic measurements were carried out by using a Quantum Design superconducting quantum interference device (SQUID) magnetometer (LakeShore 7307).

Supporting Information (see footnote on the first page of this article): To shed light on the growth process of the hierarchical Co structures, we studied the products (obtained after different periods of solvothermal treatment at 200 °C). Figures S1, S2, and S3 are low-magnification and high-magnification FESEM images of the as-synthesized S1, S2, and S3 samples collected after solvothermal reactions for 6 h and 12 h, respectively.

Acknowledgments

We acknowledge support by the Basic Research Expenses for the Special Funds of Jilin University.

[1] M. Zheng, L. Menon, H. Zeng, Y. Liu, S. Bandyopadhyay, R. D. Kirby, D. J. Sellmyer, *Phys. Rev. B* **2000**, *62*, 12282–12286.
[2] K. Liu, K. Nagodawithana, P. C. Searson, C. L. Chien, *Phys. Rev. B* **1995**, *51*, 7381–7384.
[3] V. Tzitzios, D. Niarchos, M. Gjoka, N. Boukos, D. Petridis, *J. Am. Chem. Soc.* **2005**, *127*, 13756–13757.
[4] D. Weller, A. Moser, *IEEE Trans. Magn.* **1999**, *35*, 4423–4439.
[5] P. Gambardella, S. Rusponi, M. Veronese, S. S. Dhesi, C. Grazioli, A. Dallmeyer, I. Cabria, R. Zeller, P. H. Dederichs, K. Kern, C. Carbone, H. Brune, *Science* **2003**, *300*, 1130–1133.
[6] K. T. Nam, D. W. Kim, P. J. Yoo, C. Y. Chiang, N. Meethong, P. T. Hammond, Y. Chiang, A. M. Belcher, *Science* **2006**, *312*, 885–888.
[7] Azarian, A. I. Zad, A. Dolati, *Opt. Commun.* **2007**, *274*, 471–476.
[8] J. Li, J. Huang, Y. Qin, F. Ma, *Mater. Sci. Eng. B* **2007**, *138*, 199–204.
[9] L. L. Welbes, R. C. Scarrow, A. S. Borovik, *Chem. Commun.* **2004**, *22*, 2544–2545.
[10] V. F. Puntes, K. M. Krishnan, A. P. Alivisatos, *Science* **2001**, *291*, 2115–2117.
[11] B. Q. Xie, Y. Qian, S. Zhang, S. Fu, W. Yu, *Eur. J. Inorg. Chem.* **2006**, 2454–2459.
[12] H. Cao, Z. Xu, H. Sang, D. Sheng, C. Tie, *Adv. Mater.* **2001**, *13*, 121–123.
[13] Q. Xie, Z. Dai, W. W. Huang, J. B. Liang, C. L. Jiang, Y. T. Qian, *Nanotechnology* **2005**, *16*, 2958–2962.
[14] M. H. Pan, H. Liu, J. Z. Wang, J. F. Jia, X. Q. K. Xue, J. L. Li, S. Qin, U. M. Mirsaidov, X. R. Wang, J. T. Markert, Z. Zhang, C. K. Shih, *Nano Lett.* **2005**, *5*, 87–90.
[15] Y. J. Zhang, Q. Yao, Y. Zhang, *Cryst. Growth Des.* **2008**, *8*, 3206–3212.
[16] L. P. Zhu, H. M. Xiao, W. D. Zhang, Y. Yang, S. Y. Fu, *Cryst. Growth Des.* **2008**, *8*, 1113–1118.
[17] S. R. C. Vivekchand, G. Gundiah, A. Govindaraj, C. N. R. Rao, *Adv. Mater.* **2004**, *16*, 1842–1845.
[18] W. W. Ma, Y. Yang, C. T. Chong, A. Eggeman, S. N. Piramanayagam, T. J. Zhou, T. Song, J. P. Wang, *J. Appl. Phys.* **2004**, *95*, 6801–6803.
[19] H. Cao, L. Wang, Y. Qiu, Q. Wu, G. Wang, L. Zhang, X. Liu, *ChemPhysChem* **2006**, *7*, 1500–1504.
[20] M. Knez, A. M. Bittner, F. Boes, C. Wege, H. Jeske, E. Mai, K. Kern, *Nano Lett.* **2003**, *3*, 1079–1082.
[21] H. Wu, R. Zhang, X. Liu, D. Lin, W. Pan, *Chem. Mater.* **2007**, *19*, 3506–3511.
[22] Q. Y. Liu, X. H. Guo, Y. Li, W. J. Shen, *J. Phys. Chem. C* **2009**, *113*, 3436.
[23] E. K. Athanassiou, P. Grossmann, R. N. Grass, W. J. Stark, *Nanotechnology* **2007**, *18*, 165606–165613.
[24] Q. Xie, Y. T. Qian, S. Zhang, S. Fu, W. Yu, *Eur. J. Inorg. Chem.* **2006**, 2454–2459.
[25] L. Guo, F. Liang, X. Wen, S. Yang, L. He, W. Zheng, C. Chen, Q. Zhong, *Adv. Funct. Mater.* **2007**, *17*, 425–430.
[26] L. P. Zhu, W. D. Zhang, H. M. Xiao, Y. Yang, S. Y. Fu, *J. Phys. Chem. C* **2008**, *112*, 10073–10078.
[27] D. William, J. R. Callister, *Fundamentals of Materials Science and Engineering*, John Wiley & Sons, New York, **2001**, p. 115–117.
[28] J. L. Elechiguerra, J. R. Gasga, M. J. Yacaman, *J. Mater. Chem.* **2006**, *16*, 3906–3919.
[29] H. Colfen, S. Mann, *Angew. Chem. Int. Ed.* **2003**, *42*, 2350–2365.
[30] Z. H. Yang, J. Xu, W. X. Zhang, A. Liu, S. P. Tang, *J. Solid State Chem.* **2007**, *180*, 1390–1396.
[31] Y. Soumare, C. Garcia, T. Maurer, G. Chaboussant, F. Ott, F. Fiévet, J. Y. Piquemal, G. Viau, *Adv. Funct. Mater.* **2009**, *19*, 1971–1977.
[32] R. H. Wang, J. S. Jiang, M. Hu, *Mater. Res. Bull.* **2009**, *44*, 1468–1473.
[33] C. Burda, X. B. Chen, R. Narayanan, M. A. El-Sayed, *Chem. Rev.* **2005**, *105*, 1025–1102.
[34] P. Chai, X. Liu, Z. Wang, M. Lu, X. Cao, J. Meng, *Cryst. Growth Des.* **2007**, *7*, 2568–2575.
[35] D. H. Chen, S. H. Wu, *Chem. Mater.* **2000**,*12*, 1354–1360

Received: November 15, 2009
Published Online: March 24, 2010

